A Portable Electrochemical Microcell for Weld Inspection of Duplex Stainless Steel Tanks

L.H. Guilherme,[‡,] A.V. Benedetti,[**] and C.S. Fugivara[**]*

Electrochemical tests are well-established techniques used in corrosion studies, with the development of microcells and microcapillaries enabling localized evaluation of specific microregions of a welded joint. Until now, electrochemical studies using microcells have been performed exclusively in laboratories. Therefore, the present work presents a design of a portable electrochemical microcell for weld inspection, together with its application at an industrial site. The conceptual design and the detailed engineering of the device and its components are presented and discussed. A case study was undertaken while four aseptic tanks were being constructed from UNS S32101 lean duplex stainless steel, which was welded by a tungsten inert gas welding process with automatic feed of AWS ER2209 filler metal. The electrochemical behavior of the welded joint was evaluated by acquiring cyclic potentiodynamic polarization curves in 1 mol/L NaCl aqueous solution and double loop electrochemical potentiokinetic reactivation curves in 0.5 mol/L H_2SO_4 + 0.01 mol/L KSCN aqueous solution, for microregions of the base metal, the fusion line, and the weld metal. The results demonstrated agreement between the electrochemical parameters obtained in the laboratory and at the industrial site, with both indicating that the fusion line was the microregion most susceptible to localized corrosion. Furthermore, crevice corrosion and leaks were not evidenced in the electrochemical tests at the industrial site. Therefore, storage tanks installed at an industrial site can be efficiently inspected using the portable electrochemical microcell presented in this study.

KEY WORDS: duplex stainless steel, electrochemical tests, localized corrosion, portable electrochemical microcell, storage tank, welded joint

INTRODUCTION

Industrial sites use equipment and process piping to perform chemical processes that transform inputs into finished products. Corrosion resistance and asepsis of such infrastructure are frequently required and must be evaluated at different times, as established in the production flowcharts used in sectors including the pharmaceutical and cosmetic, chemical and petrochemical, nuclear, beverage, food, and biotechnology industries.[1-4] Storage tanks are widely used at industrial sites because they are fundamental in chemical transformation processes, and it is common for them to be subjected to highly aggressive fluids and extreme temperatures (high and subzero).

These facilities are usually constructed using austenitic or duplex stainless steels, and studies have described the occurrence of localized corrosion in the heat-affected zone (near the fusion line) of the welded joints.[5-6] Localized corrosion may occur due to microstructural features of the welded joint (intermetallic phases such as chromium carbide, sigma phase, chi phase, and chromium nitride) caused by the thermal welding cycle,[7-8] where a specific microregion may become more susceptible to corrosion. Storage tanks usually have large dimensions (30 m diameter and 50 m height), so they are constructed directly at the permanent installation site.

The welding procedure specifications (WPSs) used in the construction of standard storage tanks, according to the API-650 code,[9] are in accordance with ASME code section IX (qualification standard for welding procedures and welders).[10] The requirements of ASME code section IX for qualification of a welding procedure focus on mechanical properties (tensile test, guided bend test, and radiography) and do not evaluate the performance of the welded joint in a corrosive environment. Therefore, it is possible to use a qualified WPS, according to ASME IX, that results in a welded joint with unsatisfactory metallurgical features in terms of corrosion resistance or asepsis requirements.

Another important point concerning the construction of storage tanks is related to the limitations of quality control techniques for weld inspection, in the case of applications requiring corrosion resistance or asepsis. Radiographic and ultrasonic weld inspection, liquid penetration, and magnetic particle testing are the nondestructive tests (NDTs) often used,[9,11] while the monitoring of welding focuses on the control of welding electrical parameters and the interpass temperature.[10] Therefore, the NDTs are directed toward the physical properties of the welded joint, and welding monitoring does not ensure avoidance of undesirable heat inputs that could result in an unsatisfactory microstructure of the welded joint for applications under corrosive or aseptic conditions. None of the NDTs cited is able to evaluate the influence of the microstructure on corrosion resistance.

It is evident that the inspection techniques do not evaluate the physicochemical interaction of a process or equipment with the environment to which it will be exposed. The application

Submitted for publication: August 1, 2018. Revised and accepted: December 13, 2018. Preprint available online: December 14, 2018, https://doi.org/10.5006/3004.
‡ Corresponding author. E-mail: lh.guilherme@soudap.com.br.
* Engineering Department, Soudap Engineering Company, 14802-560 Araraquara, SP, Brazil.
** Chemistry Institute, São Paulo State University (Unesp), 14800-900 Araraquara, SP, Brazil.

ISSN 0010-9312 (print), 1938-159X (online)

of electrochemical techniques provides a way to precisely evaluate this interaction, in order to provide data on the corrosion resistance and the passivation capacity of stainless steel. Electrochemical tests are well-established techniques used in studies of corrosion and passivation of stainless steels.[12-15] The use of a micrometric exposed surface area (wetted area) enables more precise evaluation of the electrochemical behavior of welded joints.[16-17] State-of-the-art techniques include microcells installed on the objective lens of an optical microscope, with coupling between the microcapillary and the sample.[18-29] Other proposals for microcell design have been described in the literature.[30-31] However, no portable electrochemical microcell systems have been reported that are suitable for weld inspection of equipment installed at an industrial site.

Therefore, this work presents the conceptual design and detailed engineering of a portable electrochemical microcell suitable for use in welding inspection at industrial sites. A case study was performed at an industrial plant, in order to evaluate the efficacy of the portable electrochemical microcell used during the construction of aseptic tanks using UNS S32101 alloy. This enabled the comparison of electrochemical parameters obtained using an electrochemical microcell in the laboratory and at the industrial site.

PORTABLE MICROCELL TECHNIQUE

A portable electrochemical microcell system for weld inspection of storage tanks was manufactured, as illustrated schematically in Figure 1. The case study focused on welding of the tank bottom plate and the assessments of the welds were made in the flat groove position (1G), according to the classification code.[10,32] The custom-built apparatus positioned the microcell parallel to the surface and enabled displacement of the microcell with a resolution of 0.001 mm (Figure 2). The coupling of the microcapillary on the tank surface was assisted by remote viewing using a digital microscope. All inspection components were organized in a suitcase in such a way as to minimize the test setup time and the duration of activities within the confined space (inside the tank).

The body of the microcell was constructed from PTFE, with dimensions of 15.0 mm × 50.0 mm (diameter vs. height) and an electrolyte volume of 3 mL. The arrangement included a platinum counter electrode and a silver|silver chloride|3 mol/L potassium chloride (Ag|AgCl|KCl 3 mol/L) reference electrode. The bottom plate of the tank was the working electrode. It is important to highlight the short distance between the electrodes (less than 5.0 mm). The diameter of the exposed test area was defined by the inner diameter of an aseptic O-ring located at the bottom tip of the microcell, which had a diameter of 1.0 mm (giving an area of 0.00785 cm^2). After demarcating the microregion to be inspected, the microcapillary was coupled to the plate surface. The welding thermal cycle normally causes a distortion in the welded joint, so an angular correction (x and y axes) was required, using the base of the microcell holder. After coupling the microcapillary, the electrolyte was added into the microcell body, up to the solution level indicator, in order to ensure the same volume for each test (ratio of 0.382 L/cm^2). The cell roof was then assembled, hence sealing the system. After each test, the aseptic O-ring and the solution were discarded, and the microcell body was washed with alcohol and dried with hot air. All the manipulations of the microcell and the microcapillary were performed using nitrile gloves and plastic tweezers, in order to avoid any possibility of contamination. The step-by-step procedure is shown in Figure 2.

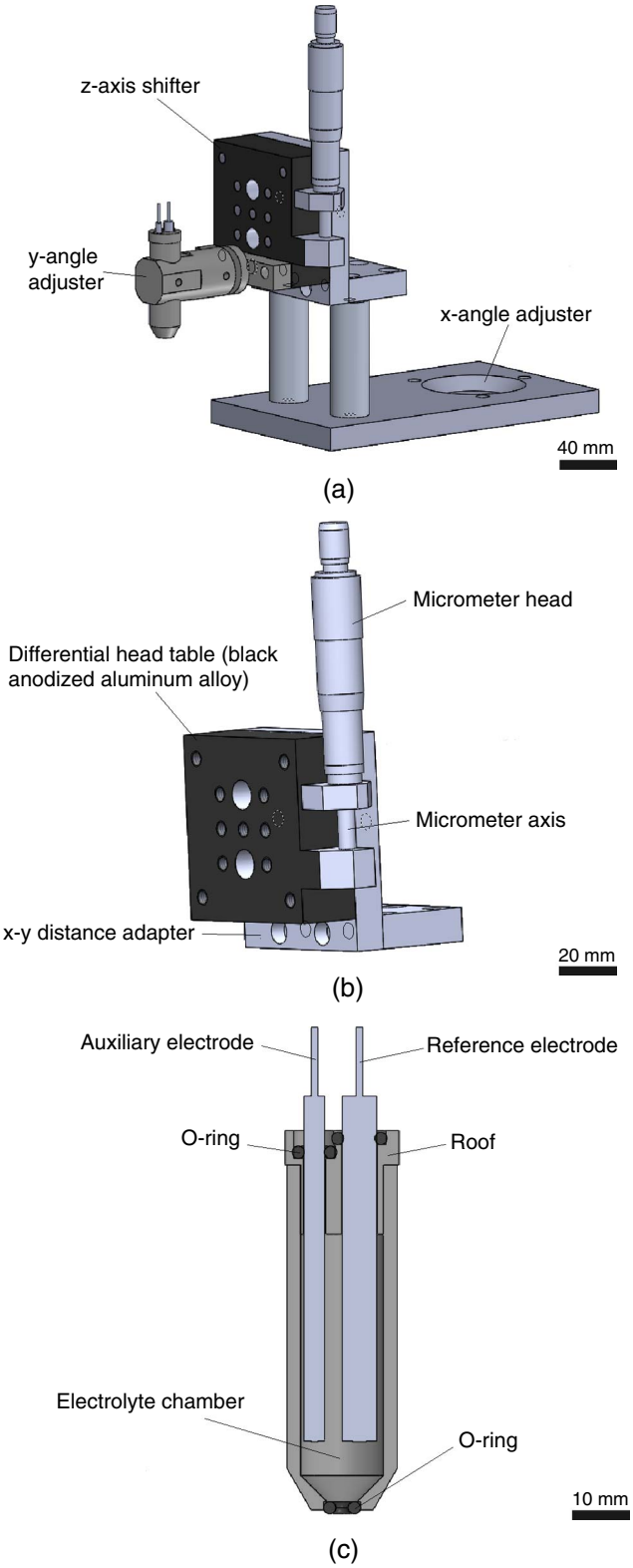

FIGURE 1. *Portable electrochemical microcell and its parts, showing (a) 3D design, (b) z-axis shifter using a sliding stage micrometer, and (c) microcell body section.*

The aseptic O-ring prevented entry of atmospheric air and allowed the formation of a thin film of electrolyte between the microcapillary and the working electrode, avoiding crevice

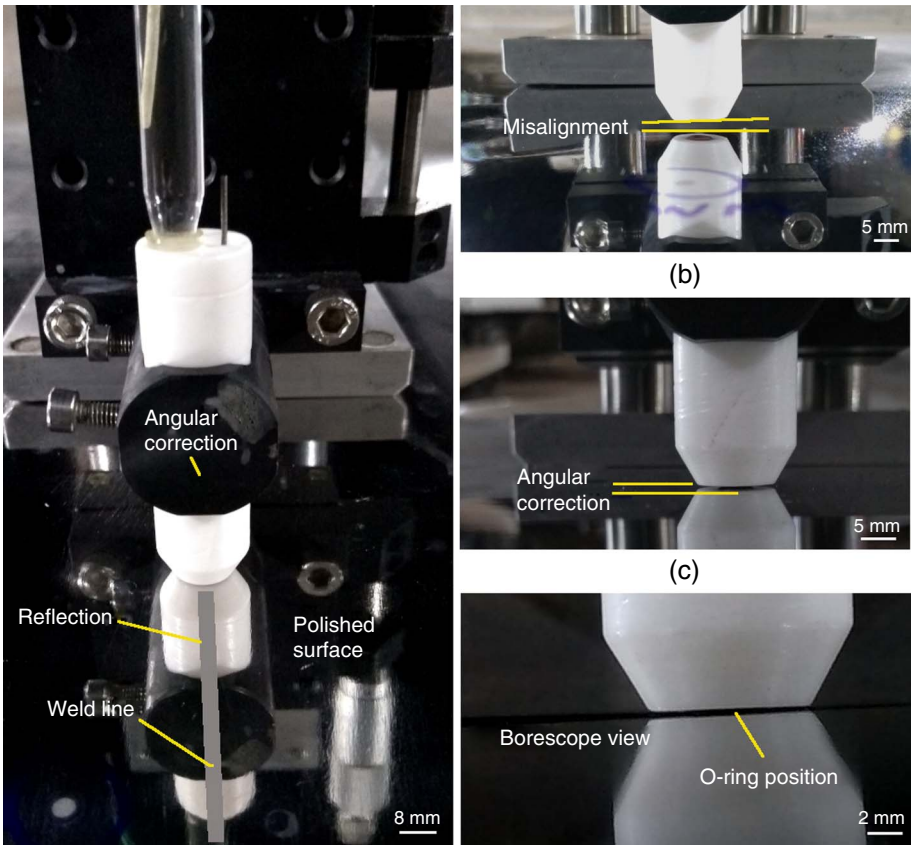

FIGURE 2. *Electrochemical testing at the industrial site, showing (a) general view of the microcell positioned on the face of the weld and the y-axis angular correction device, (b) angular misalignment between the microcapillary and the plate, due to welding distortion, (c) angular correction of the y-axis, and (d) coupling of the microcapillary on the welded joint.*

corrosion. The optical microscopy analysis of the wetted area demonstrated the absence of crevice corrosion and the reproducibility of the exposed test area. Figure 3 shows micrographs of the wetted area, after acquisition of the potentiodynamic polarization curves, obtained using a digital microscope for the tests performed at the industrial site (Figures 3[a] and [b]), and by optical microscopy for the tests performed in the laboratory (Figures 3[c] and [d]). The electrochemical tests were performed under two potential range conditions, in order to evaluate the occurrence of crevice corrosion around the microcapillary: (i) $E_{end} = E_{pit} + 100$ mV and (ii) $E_{end} = 1.2$ V.

MICROCELL STUDIES AT THE INDUSTRIAL SITE

The case study was performed during the construction of four orange juice storage tanks installed inside a cold storage warehouse. Each tank had a capacity of 9,465 m^3, diameter of 21 m, and height of 32 m. The storage tanks were constructed using a lean duplex stainless steel alloy with plate specification to coil finish 2B (Ra < 0.8 µm), and were welded using a tungsten inert gas (TIG) process. The classification of the tanks was in accordance with API 650,[9] ASME VIII,[11] and ASME BPE,[3] where the equipment is defined as food grade and is submitted to a corrosive environment. After 3 y of operation, the maintenance record indicated that localized corrosion occurred in the weld fusion line of the tank bottom plate.

The chemical compositions of the materials studied (UNS S32101 and AWS ER2209) are shown in Table 1. The base metal (UNS S32101) was received as a coil 6 mm thick, and the weld metal used was AWS A5.9 ER2209 welding wire with diameter of 1.2 mm. The WPS for the tank bottom joints used a single V groove joint, with the same base material being used as a backing plate. The WPS applied four bead welds for the multiple-pass layers, as shown schematically in Figure 4. The TIG welding process with automatic wire feed was performed with a welding machine (EWM Tetrix 351 Comfort FW) in the flat position, using the electrical parameters shown in Table 2.

The heat input was calculated using Equation (1),[10] with values between 1.34 kJ/mm and 2.31 kJ/mm being obtained:

$$E = \frac{A \cdot V}{v_s} \quad (1)$$

where E is the heat input (kJ/mm), v_s is the average welding speed (mm/min), A is the current (A), and V is the voltage (V).

The electrochemical tests were performed under two conditions: (1) using the portable microcell at the industrial site and (2) applying standard laboratory testing procedures. This protocol enabled comparison of the electrochemical parameter values obtained at the industrial site with those obtained in the standard laboratory tests. Cyclic potentiodynamic polarization (CPP) and double loop electrochemical potentiokinetic reactivation (DL-EPR) were performed, with a capillary (internal diameter of 1.0 mm) used for measurements in the weld microregions under both test conditions, as shown in Figure 4. The microregions assessed for each weld were classified as (i) base metal, (ii) weld face, and (iii) fusion line. Ten measurements

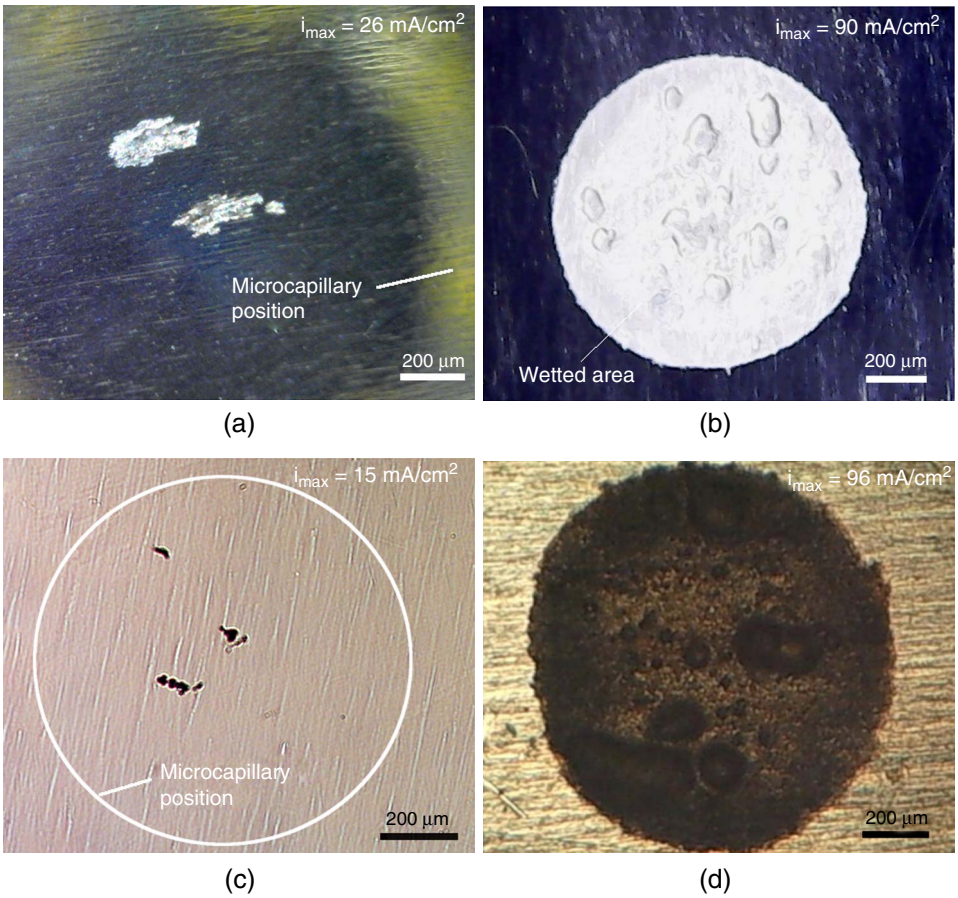

FIGURE 3. *Micrographs of the wetted area (0.00785 cm^2), free of crevice corrosion, observed using (a) digital microscopy at the industrial site, with $E_{end} = E_{pit} + 100$ mV, (b) digital microscopy at the industrial site, with $E_{end} = 1.2$ V, (c) optical microscopy in the laboratory, with $E_{end} = E_{pit} + 100$ mV, and (d) optical microscopy in the laboratory, with $E_{end} = 1.2$ V/Ag\|AgCl\|KCl 3 mol/L.*

of each test type were made in each microregion, and all the measurements were performed at room temperature (25°C). A Palmsens v. 3 potentiostat was operated using commercial PSTrace v. 3.4 software. Additionally, CPP and DL-EPR tests were performed on one fusion line after a weld repair. It is common for pores to appear during weld reinforcement grinding, with such nonconformity regions then being repaired by welding. The electrochemical tests assessed the effect of the welding thermal cycle in the fusion line microregion.

In the electrochemical tests performed at the industrial site, the microcapillary was coupled to the weld face, as the tank bottom plates were assembled on a concrete base and the V bevel was consequently only welded on one side. Preparation of the surface at the industrial site was performed using a portable pneumatic grinder (type AT-7033, PUMA) to remove the weld reinforcement, grinding with up to 600 grit sandpaper, and polishing with diamond suspensions (20 µm, 10 µm, and 6 µm). A digital portable rugosimeter (type SJ-210, Mitutoyo) was used to measure the average roughness (Ra), with resolution of 0.050 µm.

Standard laboratory testing procedures were performed using a mock-up weld (similar to the WPS used for the tank bottom joint) produced in accordance with the welding procedure qualification codes.[10,31] The welding parameters are described in Table 2. A standard microcell and microcapillary[16] were used for the electrochemical testing of the welded joint microregions (Figure 4). The sample was mounted in polyester cold cure resin, mechanically sanded with up to 600 grit sandpaper, and polished with diamond suspensions (20 µm, 10 µm, and 6 µm).

The degree of sensitization (DOS) of the welds was measured using the DL-EPR test in 0.5 mol/L H_2SO_4 + 0.01 mol/L KSCN solution. The open circuit potential (OCP) was measured for 5 min to ensure that it was stabilized. The potential was scanned in the anodic direction, from −500 $mV_{Ag/AgCl}$ to +300 $mV_{Ag/AgCl}$, after which the polarization scan was reversed in the cathodic direction, up to −500 $mV_{Ag/AgCl}$. A sweep rate of 1.67 mV/s was used and the DOS was evaluated in terms of the charge ratio ($(Q_r/Q_a) \times 100$).

Table 1. *Chemical Compositions (wt%) of UNS S32101 and ER 2209*

	Elements (wt%)									
Sample	**C**	**Cr**	**Ni**	**Mo**	**Mn**	**P**	**S**	**Si**	**N**	**Cu**
UNS S32101	0.019	21.32	1.15	0.19	4.87	0.024	0.001	0.73	0.22	0.53
ER 2209	0.020	22.90	8.6	3.20	1.6	0.017	0.001	0.4	0.16	0.10

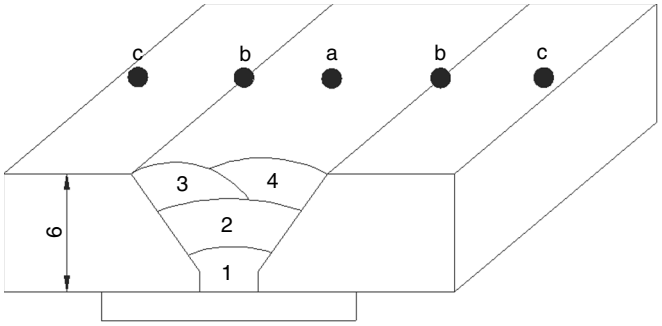

● Microcapillary coupling

a Weld face

b Fusion line

c Base metal

FIGURE 4. *Schematic illustration of the welded joint, showing detail of the bevel, the passes of the weld, and the microcapillary coupling points.*

Table 2. *Welding Conditions*[(A)]

Weld Pass	Current (A)	Voltage (V)	Travel Speed (mm/s)	Heat Input (kJ/mm)
1	121±1	16.0±0.4	1.43±0.1	1.34±0.2
2	140±1	15.1±0.3	0.91±0.1	2.31±0.1
3	142±1	15.8±0.5	1.49±0.1	1.52±0.1
4	142±1	15.8±0.5	1.36±0.1	1.65±0.1

[(A)] Current, voltage, and speed variations were registered during welding. Contact tip to work distance (CTWD): ±10 mm. Shielding gas/flow rate/Polarity: 100% Ar/15 L/min/DCEN(−).

Cyclic polarization tests in 1.0 mol/L NaCl solution were used to evaluate the pitting corrosion resistance. After stabilization of the OCP (5 min), an anodic polarization scan was performed at a sweep rate of 1.67 mV/s. The anodic scan was reversed at a current density of 1 mA/cm^2, with the sample then being scanned in the cathodic direction to a potential of −200 mV$_{OCP}$.

RESULTS

Figure 5 shows the DL-EPR curves obtained in 0.5 mol/L H_2SO_4 + 0.01 mol/L KSCN solution, for the standard laboratory tests and the industrial site tests.

CPP curves for the weld microregions in 1 mol L^{-1} NaCl solution are presented in Figure 6. All the polarization curves followed Tafel-type behavior, with no evidence of the active current peak when the potential was anodically scanned, showing that all the microregions had been previously passivated due to the oxide film formed in an air atmosphere.[33] Figure 7 shows the corrosion potential (E_{corr}), pitting potential (E_{pit}), protection (or repassivation) potential (E_{rp}), passive region ($E_{rp} - E_{corr}$), and DOS.

DISCUSSION

It can be seen in Figure 5 that the fusion line microregions presented a large reactivation peak in the cathodic scan (Figure 5[c]), which increased after the weld repair procedure (Figure 5[d]). For duplex stainless steels, the peak observed in the cathodic scan has been attributed to preferential corrosion attack in Cr-depleted regions (around carbide and nitrides of Cr, sigma phase, α', G, and other Cr-rich phases).[34-36] As shown in Figures 5(a) and (b), there was a clear difference between the LDSS 2101 base metal and the ER2209 weld metal, in terms of the anodic peak current density. This difference was related to the higher contents of the alloying elements Cr, Ni, and Mo in the weld metal (although there was dilution with the base metal). Due to the difference in chemical composition, the ER2209 filler metal presents a higher pitting resistance equivalent number (PREN) than UNS S32101. The PREN method is used to classify duplex stainless steels as a function of the localized corrosion resistance (pitting and intergranular corrosion), with a higher PREN indicating greater resistance to localized corrosion.[37] In this study, the PREN of the base metal was 26 and that of the filler metal was 36.[38]

At the industrial site tests, lower pitting potential was observed for the base metal and the fusion line microregion, compared to the standard laboratory tests (Figure 6). This difference in electrochemical behavior was due to the residual stress and cold working during assembly of the plates, as reported previously.[39-40] The fusion line microregion presented the least noble electrochemical behavior, and it was observed that the corrosion resistance decreased after the weld repair procedure (Figure 6[d]). This could be attributed to local segregation and the depleted zone along the fusion line of LDX 2101 welds, as described in the literature.[34] Furthermore, the $E_{rp} - E_{corr}$ value was higher for the weld face, compared to the other microregions. This was indicative of higher stability of the passive layer formed on the weld face, revealing that it had the lowest tendency for pitting corrosion among all the microregions.

In general, the weld face microregion exhibited higher values of corrosion resistance than the LDSS 2101 base metal, and this is related to the PREN values of each microregion, which are 26 and 36 to the base metal and the weld face, respectively. The fusion line microregion showed the lowest corrosion and pitting potentials, and the weld face showed higher values of E_{pit} than fusion line, due to higher filler metal dilution for fusion line. The filler metal ER2209 have higher Ni content than the base metal and the presence of Mo. Nickel stabilizes austenite, while molybdenum stabilizes ferrite and provides to increase the PREN of ferrite. Tan, et al.,[7,41] studied a super duplex stainless steel and reported that the pitting corrosion resistance was defined by the PREN of the weaker phase. If the PREN of the weaker phase increases, the global corrosion resistance of steel increases as well. It is noteworthy that the fusion line shows a higher proportion of ferrite than weld face, and the nitride precipitation is also more likely to occur in the ferrite phase. Several authors[7,42-46] reported that the fusion line microregion was the preferential site for pits nucleation due to possible chromium nitride particles.

The welding thermal cycle of the WPS exposed the fusion line microregion to the temperature range in which the precipitation of the surface defects sites occurs (e.g., Cr_2N precipitates),[7] and these local defects are the culprits by the lowest corrosion resistance. Some authors[7,17,47] showed that the nitride colonies precipitated in the interior of a ferrite grain in the HAZ, near the weld metal, where these depleted zones have an average size of around 20 μm–100 μm and the spacing among these local defects can be lower than 50 μm. Therefore, it is important to point out that the coupling protocol of the capillary

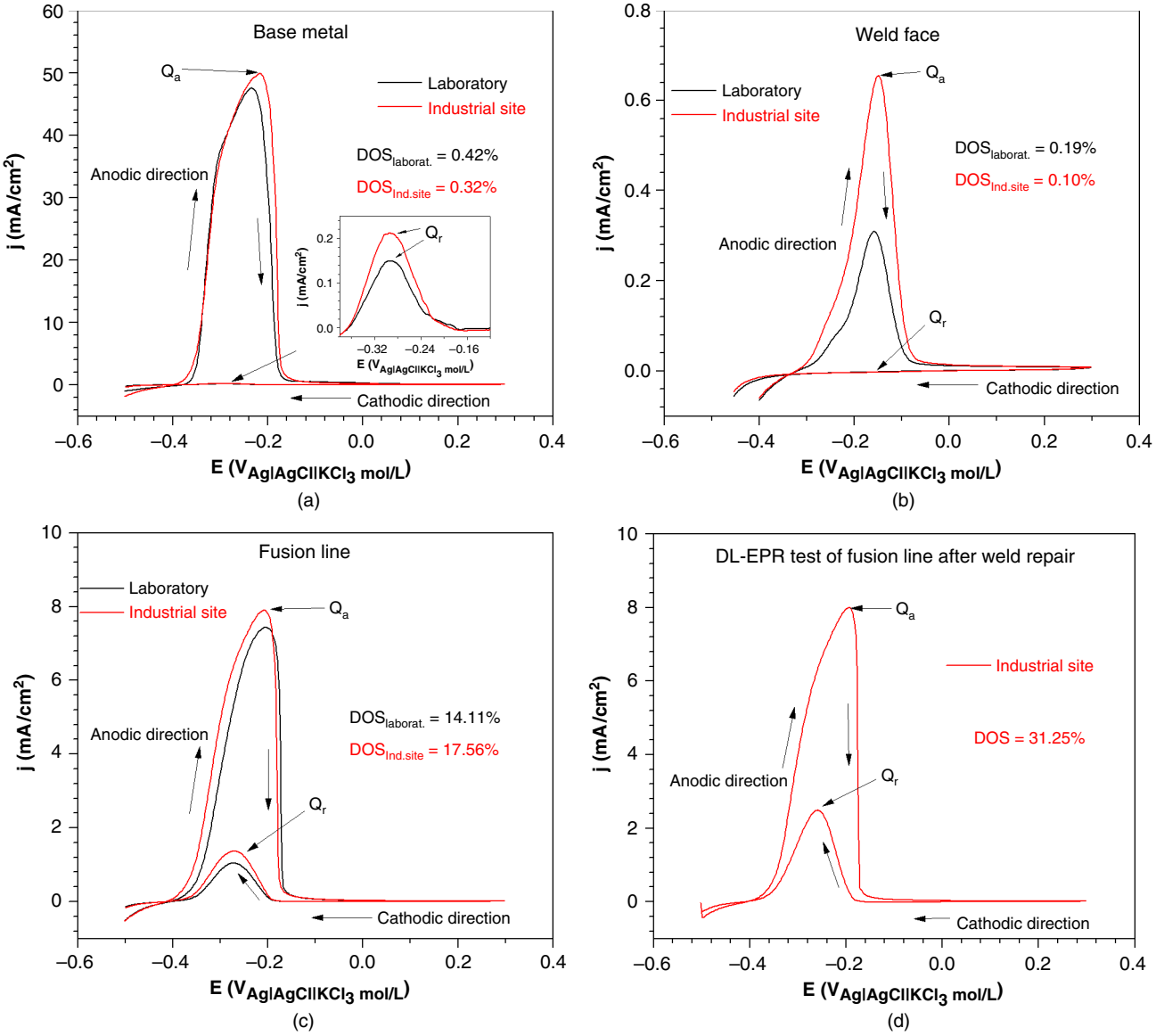

FIGURE 5. *DL-EPR curves for the base metal and weld microregions at 25°C. Solution: 0.5 mol/L H_2SO_4 + 0.01 mol/L KSCN; area of the working electrode = 0.00785 cm^2; and scan rate: 1.67 mV/s. Investigated microregions were (a) base metal, (b) weld face, (c) fusion line, and (d) fusion line after weld repair procedure.*

on the fusion line microregion (as shown in Figure 4) makes it possible to perform the electrochemical tests on the surface containing these local defects, as the area of capillary is 0.785 mm^2.

The size of the capillary was suitable to differentiate the electrochemical behavior of each microregion investigated, and to obtain specific corrosion resistance parameters as a function of the microregion. It is highlighted that the results were reproducible and low standard deviations were observed, as shown in Figure 7. The E_{pit} and DOS were the electrochemical parameters more sensitive to detect the differences between the microregions. The base metal and the weld face microregions demonstrated lower standard deviations to the corrosion resistance parameters than fusion line microregion probably because those microregions have homogeneous microstructures without Cr-depleted zones. The fusion line microregion exhibited higher standard deviations, and these variations occurred as a function of the number of chromium-depleted zones present on the scanned surface area.

Ten measurements of each test type were made in each microregion and the variability of the results can be analyzed based on the coefficient of variation (CV), which is a measure of dispersion of data relative to the mean. It is defined as the standard deviation divided by the mean. It is important to point out that all electrochemical parameters of the microregions shown in Figure 7 obtained low CV, and this performance is exemplified by the CV values of pitting potential: base metal (4.8%), weld face (2.1%), and fusion line (12.5%). Therefore, the portable microcell and its inspection procedure have really represented the electrochemical behavior of each microregion.

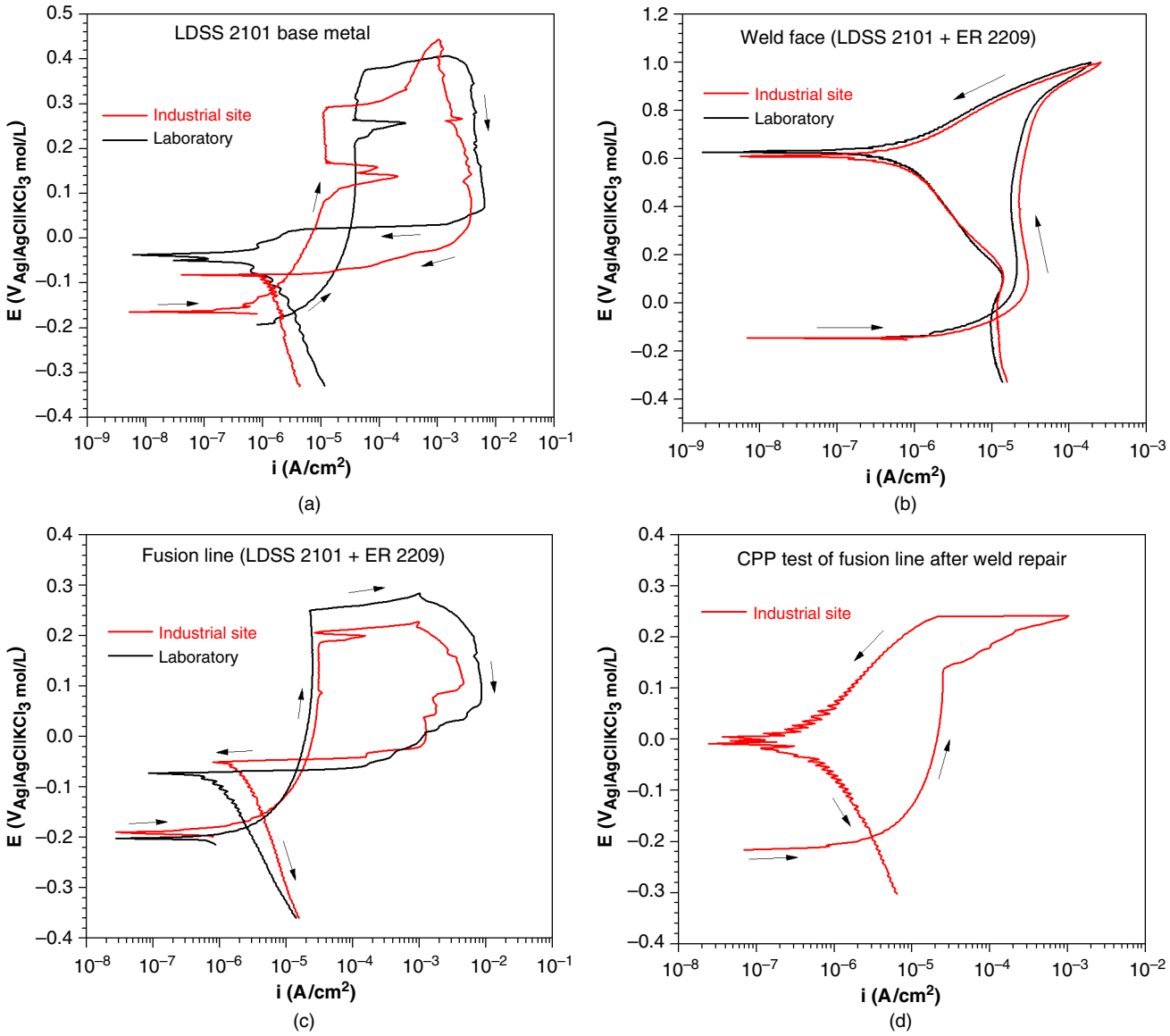

FIGURE 6. *CPP curves for the base metal and weld microregions at 25°C. Solution: 1.0 mol/L NaCl; area of the working electrode = 0.00785 cm^2; and scan rate: 1.67 mV/s. Investigated microregions were (a) base metal, (b) weld face, (c) fusion line, and (d) fusion line after weld repair procedure.*

The results demonstrated that the portable microcell could be used to satisfactorily evaluate the electrochemical behavior of the tank welds, as the results obtained in the field were similar to the standard laboratory test results. Until now, although weld mechanical properties are widely investigated by nondestructive testing (NDT), the aseptic and corrosion properties have not been investigated, due to the absence of suitable instrumentation. Now, the portable microcell makes it possible to investigate the corrosion resistance and aseptic properties of equipment in the construction phase and during its life cycle (in planned maintenance procedures). Another application of the portable microcell is selection of the best welding parameters for a typical welded joint, according to the WPS. The WPS specifies a wide range of welding parameters for each type of welded joint, so welders can apply different welding conditions that result in distinct electrochemical behaviors for the same type of welded joint. The portable microcell can be used to select the best welding parameters by means of electrochemical tests on weld mock-up samples at the construction site. Hence, it is possible to configure the welding machine program so that all welds are performed using the same welding parameters that result in the best corrosion resistance. Therefore, the portable electrochemical microcell constitutes a powerful tool for use in predictive maintenance activities involving equipment installed at an industrial site.

It is important to point out that this version of the portable microcell is limited to the inspection of welds in a flat position, due to the nature of the holder and the z-axis shifter. Another limitation is the need for grinding of the exposed surface area after the electrochemical testing of equipment, as the mark left by the assay (DL-EPR) should be removed. Two main kinds of equipment are normally evaluated: one normally finished with 220 grit (e.g., tanks to storage orange juice) and another

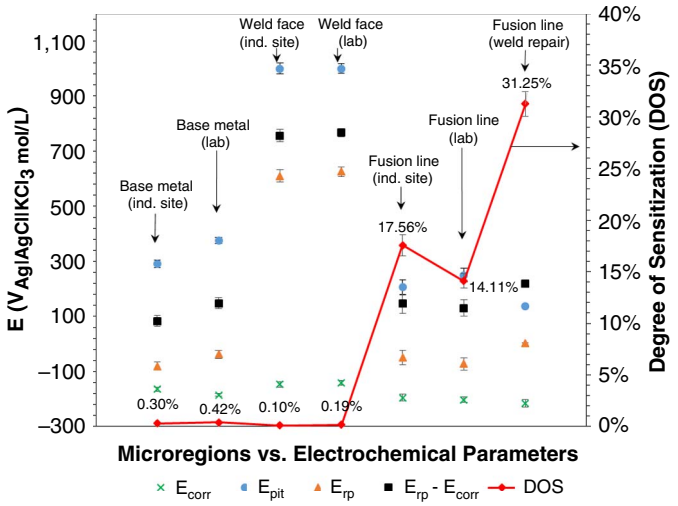

FIGURE 7. *Quantitative determination of electrochemical parameters in the CPP and DL-EPR tests. Error bars represent the standard deviation of the mean value.*

electropolish finish (e.g., tanks used in pharmaceutical industry). The first group of equipment can be evaluated using the portable microcell, due to the surplus metal from grinding. On the other hand, evaluation using the portable microcell is not appropriate for equipment with electropolished surfaces, as the assay mark removal may change the equipment standard condition. In such cases, the inspection of a weld mock-up sample is recommended.

CONCLUSIONS

➢ The design presented in this study resulted in a robust and versatile portable electrochemical microcell. An optimized setup time for executing the electrochemical tests showed that the microcell is a good option for the inspection of duplex stainless steel tanks. Adequate sensitivity for data acquisition was observed for the circuit formed between the portable microcell and the components, with electrochemical parameters obtained at the industrial site agreeing with those obtained in the standard laboratory tests. The electrochemical parameters obtained at the industrial site were reproducible and enabled differentiation of the microregions of the welded joint, as a function of the electrochemical response. The fusion line presented the lowest corrosion resistance among all the microregions assessed. The maintenance records of the tanks in operation showed that the fusion line was the microregion most susceptible to localized corrosion, corroborating the results obtained with the portable microcell. Therefore, the findings of the present study demonstrate that it is possible to use a portable electrochemical microcell for the purpose of quality control of tanks installed at an industrial site. There is, however, the need to further improve understanding of the electrochemical behavior observed using the portable microcell at an industrial site, using other electrochemical techniques and electrolytes.

ACKNOWLEDGMENTS

The authors would like to thank the São Paulo Research Foundation (FAPESP) for providing financial support for this research (Proc. No. 2016/08439-0).

References

1. W.M. Huitt, B.K. Henon, V.B. Molina, *Chem. Eng.* 118 (2011): p. 49-53.
2. G.J. Farquharson, "Hygienic Equipment and Systems—Regulations, Issues, Standards and Good Practice," *VTT Symposium* (Valtion Tek. Tutkimuskeskus, 2003).
3. W.M. Huitt, *PDA J. Pharma. Sci. Technol.* 65 (2011): p. 81-90.
4. L.H. Guilherme, C.A. Della Rovere, S.E. Kuri, M.F. de Oliveira, *Weld. Int.* 30 (2016): p. 268-276.
5. A.I. Karayan, H. Castaneda, *Eng. Fail. Anal.* 44 (2014): p. 351-362.
6. J. Huang, B. Han, G. Liu, M. Yan, X. Zhu, *Corros. Sci. Prot. Technol.* 13 (2001): p. 526-530.
7. D.C. Sicupira, R.C. Junior, A.Q. Bracarense, G.S. Frankel, V.F. Cunha Lins, *Mater. Res. J. Mater.* 20 (2017): p. 161-167.
8. G. Mohammed, M. Ishak, S. Aqida, H. Abdulhadi, *Metals (Basel)* 39 (2017): p. 1-18.
9. API standard (650), "Welded Steel Tanks for Oil Storage," (API Standard, 1966).
10. ASME-IX, "Welding, Brazing, and Fusing Qualifications," (ASME Boiler Pressure and Vessel Code, 2015).
11. ASME-VIII, "Rules for Construction of Pressure Vessels: Division 1 & 2," (ASME Boiler and Pressure Vessel Code, 2010).
12. A.J. Sedriks, *Corrosion of Stainless Steels*, 2nd ed. (New York: Wiley-Interscience, 1996).
13. R. Magnabosco, N. Alonso-Falleiros, *Corrosion* 61 (2005): p. 130-136.
14. I.H. Lo, Y. Fu, C.J. Lin, W.T. Tsai, *Corros. Sci.* 48 (2006): p. 696-708.
15. A. Turnbull, P.E. Francis, M.P. Ryan, L.P. Orkney, A.J. Griffiths, B. Hawkins, *Corrosion* 58 (2002): p. 1039-1048.
16. F. Andreatta, L. Matesanz, A.H. Akita, L. Paussa, L. Fedrizzi, C.S. Fugivara, J.M. Gómez de Salazar, A.V. Benedetti, *Electrochim. Acta* 55 (2009): p. 551-559.
17. D.C. Sicupira, G.S. Frankel, V. de F.C. Lins, *Mater. Corros.* 67 (2016): p. 440-448.
18. L.C. Abodi, O. Dolgikh, H. Terryn, J. Deconinck, *Electrochim. Acta* 189 (2016): p. 128-136.
19. F. Andreatta, L. Fedrizzi, *Electrochim. Acta* 203 (2015): p. 337-349.
20. M. Sánchez, J. Gamby, H. Perrot, D. Rose, V. Vivier, *Electrochem. Commun.* 12 (2010): p. 1230-1232.
21. M. Sánchez, N. Aouina, D. Rose, P. Rousseau, H. Takenouti, V. Vivier, *Electrochim. Acta* 62 (2012): p. 276-281.
22. F. Arjmand, A. Adriaens, *J. Solid State Electrochem.* 18 (2014): p. 1779-1788.
23. H. Böhni, T. Suter, F. Assi, *Surf. Coatings Technol.* 130 (2000): p. 80-86.
24. F. Arjmand, A. Adriaens, *Electrochim. Acta* 59 (2012): p. 222-227.
25. T. Suter, E.G. Webb, H. Böhni, R.C. Alkire, *J. Electrochem. Soc.* 148 (2001): p. 174-185.
26. T. Suter, H. Böhni, *Electrochim. Acta* 43 (1998): p. 2843-2849.
27. H. Böhni, T. Suter, A. Schreyer, *Electrochim. Acta* 40 (1995): p. 1361-1368.
28. M.M. Lohrengel, A. Moehring, M. Pilaski, *Electrochim. Acta* 47 (2001): p. 137-141.
29. F. Andreatta, M.M. Lohrengel, H. Terryn, J.H.W. De Wit, *Electrochim. Acta* 48 (2003): p. 3239-3247.
30. T. Suter, H. Bohni, *Electrochim. Acta* 47 (2001): p. 191-199.
31. A.M. Panindre, K.H. Chang, T. Weirich, G.S. Frankel, *Corrosion* 74 (2018): p. 847-850.
32. AWS D1.1, "Structural Welding Code-Steel," (American Welding Society, 2010).
33. W. Li, J. Luo, *Electrochem. Commun.* 1 (1999): p. 349-353.
34. E.M. Westin, "Microstructure and Properties of Welds in the Lean Duplex Stainless Steel LDX 2101," (Doctoral Thesis, School of Industrial Engineering and Management, Royal Institute of Technology, Stockholm, 2010).
35. R. Silva, L.F.S. Baroni, M.B.R. Silva, C.R.M. Afonso, S.E. Kuri, C.A.D. Rovere, *Mater. Charact.* 114 (2016): p. 211-217.
36. E.B. Mélo, R. Magnabosco, C. de Moura Neto, *Mater. Res.* 16 (2013): p. 1336-1343.
37. Z. Zhang, H. Jing, L. Xu, Y. Han, L. Zhao, C. Zhou, *Appl. Surf. Sci.* 404 (2017): p. 110-128.
38. F.V.V. Sousa, M.C.E. Bandeira, O.R. Mattos, C.J.B.M. Joia, F.P. Dos Santos, "Laboratory Test to Evaluate Lean Duplex UNS S32101 and UNS S32304 Flexible Pipe Carcass at Sour Service," NACE—International Corrosion Conference Series (New Orleans, U.S.A.: NACE, 2017).

39. ASM International, *ASM Handbook*, vol. 13 (Materials Park, OH: ASM International, ASM, 1992).
40. C. Örnek, D.L. Engelberg, *Corros. Sci.* 99 (2015): p. 164-171.
41. H. Tan, Y. Jiang, B. Deng, T. Sun, J. Xu, J. Li, *Mater. Charact.* 60 (2009): p. 1049-1054.
42. L. Chen, H. Tan, Z. Wang, J. Li, Y. Jiang, *Corros. Sci.* 58 (2012): p. 168-174.
43. H.Y. Ha, M.H. Jang, T.H. Lee, J. Moon, *Corros. Sci.* 89 (2014): p. 154-162.
44. H. Tan, Z. Wang, Y. Jiang, D. Han, J. Hong, L. Chen, L. Jiang, J. Li, *Corros. Sci.* 53 (2011): p. 2191-2200.
45. L. Wickström, G. Hinds, A. Turnbull, *Corrosion* 71 (2015): p. 1036-1047.
46. J. Xiong, S. Agarwala, M.Y. Tan, M. Forsyth, *Corrosion* 71 (2015): p. 1248-1256.
47. E.M. Westin, S. Hertzman, *Weld. World* 58 (2014): p. 143-160.